Compact Beam Splitters with Deep Gratings for Miniature Photonic Integrated Circuits: Design and Implementation Aspects

Chin-Hui Chen,[1,*] Jonathan Klamkin,[2] Steven C. Nicholes,[3] Leif A. Johansson,[1] John E. Bowers,[1] and Larry A. Coldren[1,3]

[1]*Department of Electrical and Computer Engineering,University of California Santa Barbara, Santa Barbara, CA, 93106, USA*

[2]*MIT Lincoln Laboratory, Lexington, MA, 02420, USA*

[3]*Department of Materials, University of California Santa Barbara, Santa Barbara, CA, 93106, USA*

[*]*Corresponding author: janet@ece.ucsb.edu*

We present an extensive study of an ultra-compact grating-based beam splitter suitable for photonic integrated circuits (PICs) which have stringent density requirements. The 10 μm long beam splitter exhibits equal splitting, low insertion loss, and also provides a high extinction ratio in an integrated coherent balanced receiver. We further present the design strategies for avoiding mode distortion in the beam splitter, and discuss the optimization of the widths of the detectors in order to improve insertion loss and extinction ratio of the coherent receiver circuit. In our study, we show that the grating-based beam splitter is a competitive technology having low fabrication complexity for ultra-compact PICs.

OCIS codes: 230.1360, 130.3120.

1. Introduction

In past few decades considerable attention has been given to waveguide beam splitters in optical integrated devices. With increasing demands on PIC performance, compactness requirements are becoming more stringent, similar to their electronic counterparts. For some applications with optical feedback circuits, such as optical phase-locked loops [1], the

system stability greatly relies on ultra-short loop delays.

Conventional directional couplers with dimensions of millimeters or more have become less attractive due to the chip size requirements. The size of a conventional surface ridge multimode interference (MMI) beam splitter is usually limited by lithographic resolution of the gap between access waveguides since the interaction length is proportional to square of its width. Moreover, long curves and S-bends are also necessary in order to separate the access beams for fiber coupling or integration with other components. Such fundamental attributes hinder the progress of device downsizing. Though significant efforts have been made to achieve interference lengths on the order of 100 μm [2–5]; these components typically pay the price of higher insertion loss and lower fabrication tolerance. Alternatively other advanced technologies such as photonic crystals [6–9] and air trenches [10, 11] have been used to construct beam splitters in the submicron range. However, the performance of these beam splitters, unfortunately, is sensitive to process variations, and their applications are limited by fabrication complexity and low throughput.

The criteria for designing an ultra-compact beam splitter must also include the relative sizes of other integrated components. In present PIC technologies, the overall device sizes and the propagation lengths in a feedback loop are still dominated by the sizes of other elements such as modulators, detectors and connecting waveguides, which are typically hundreds of microns long or more. Therefore, it is beneficial to reduce the size of the beam splitter from millimeters to several microns for the purpose of minimizing the total device footprint and the signal propagation delay, but there is only a minor improvement to advance from microns to submicron range.

In this paper we present a comprehensive study of a proposed grating-based beam splitter [12, 13] which uses a 10 μm-long ultra-compact strong interference region for equal splitting. This beam splitter is carried out by well-established and robust fabrication steps that enable potentially large throughput, and is compatible with existing integration platforms. The orientation of the splitter allows input beams to be coupled from opposing facets, which is advantageous in simplifying fiber alignment and packaging. These key advantages make the grating-based beam splitter a desirable and yet practical solution compared with other advanced technologies.

2. Beam Splitter Design

The goal of this work is to realize an integrated beam splitter with equal splitting, low insertion loss, short propagation length, as well as a high degree of interference between the incoming lights. Fig. 1(a) and 1(b) show the configuration of the compact 2×2 grating-based beam splitter with integrated modulators and photodetectors which are used in this work to obtain the data presented below.

2.A. Design Issues and Key Features

The grating region splits an incoming beam into transmissive (undiffracted) and reflective (diffracted) beams. Similar to Bragg diffraction in planar phase gratings [14], geometric and diffraction beam walk-off plus unequal mode distortion, however, arise in the case of oblique incidence of a finite beam onto a relatively thick grating region. The oblique multiple reflections from a series of grating grooves widen the reflective beams, and this widening becomes more pronounced with larger angles. On the other hand, the mode distortion is due to the continuous energy exchange between the diffracted and undiffracted beams during the interference process [14]. As a result, the interference extinction ratio between the two output beams could be severely decreased if falling into the degraded regime. Qualitatively speaking, it is important to keep the input angle near normal incidence and to arrange the beam size comparable to or wider than the grating length at the grating region.

In order to avoid the mode degradation, three design features are implemented. First, we design a quasi free space region surrounding the gratings for the purpose of expanding the beams within the shortest propagation distance. The beams diverge freely in the lateral direction without seeing the waveguide boundary and are only confined in the transverse direction in this region. Broadening a beam width wider than the grating length helps alleviate the mode distortion. We utilize a beam propagation method to simulate the mode expansion behavior in this region compared to one using a linear flaring. As shown in Fig. 2, the slope of beam widths to propagation distances in the quasi free space case is about 5 to 12 times larger than the linear cases, depending on the designated percentage of mode transfer. The beam divergence in a quasi free space region is shown to be much faster than the one in a conventional linear adiabatic tapering. This feature minimizes the traveling distance from the input waveguides to the output detectors and therefore keeps a compact device footprint and a small signal path in a feedback loop. In addition, it is also beneficial to reduce the detector front end saturation.

Second, we design input waveguides to have a small incident angle in order to eliminate

the beam walk-off. The lower bound of the incident angle is limited by the asymptotic line of the Gaussian beam divergence in the quasi free space region, which is determined by

$$\Theta \cong \frac{w(z)}{z} = \frac{\lambda}{\pi w_o}, \tag{1}$$

where $w(z)$ is the beam width at z distance along propagation, w_o is the beam waist, and λ is the beam wavelength in the waveguide. The asymptotic angle is calculated to be 2.89° in our design. Although a small incident waveguide angle helps relieve the beam walk-off effect, the trade-off is the long distance used to distinguish the beams on the same side of the gratings. A waveguide angle of 10° from normal incidence to the grating grooves is selected instead of one that close to the asymptotic angle. It is simulated to still be small enough to avoid mode distortion and to be sufficiently large to differentiate the beams within reasonably short total propagation length.

Third, we design a strongly reflective Bragg grating for 1550 nm wavelength in order to achieve the targeted reflection with an ultrashort coupling length. Fig. 3(a) illustrates the cross-section of the grating region with a maximal coupling coefficient (κ) by replacing the multiple quantum well (MQW) slab waveguide periodically with regrown InP material (Fig. 3(b)) to achieve a high reflectivity. It allows the grating grooves to interfere with the beams symmetrically in the vertical plane along the propagation direction; therefore, implies a small scattering loss. More details are given in the following paragraphs.

2.B. Models

The design principle of the grating-based beam splitter is further analyzed by both a horizontal model and a vertical FDTD model. Since in the quasi free space region the beam is only confined in the vertical (transverse) dimension, decomposing the problem into two 2-D models, horizontal (x-z plane) and vertical (y-z plane) ones, should not lose its generality but rather reduces the complexity and saves computing resources. In the horizontal model, the time monitor is used to mimic the functionality of the detector by recording the power flow along the propagation direction. We first study the case of one input with equal splitting as shown in Fig. 4(a) and 4(b). With the input beam equally bisected into transmission and reflection parts by the grating region, the second input is then introduced symmetrically in the model. Fig. 5 and Fig. 6 show the interference phenomenon resulting from the phase difference of the two input beams. The simulated numerical results are also shown in Table 1. They demonstrate that more than a 16 dB extinction ratio is theoretically achievable with the selected 10° incident angle at equal splitting.

The exact centered-MQW waveguide layer structure with a total thickness of 3695 Å is constructed in a FDTD vertical model. The radiation losses caused by different grating etch depth is studied as shown in Fig. 7. For shallow etch depths, the corrugated grating can be seen as small perturbation which is usually studied by coupled-mode theory, and its radiation loss is negligible. As the etch depth gets deeper, the mismatch increases between the unperturbed waveguide mode and the grating Bloch mode. The transverse displacement originates from the asymmetric material index that the mode experiences in the grating region. The loss passes through a maximum at an etch depth of around half the waveguide thickness, and the loss rolls off with deeper grooves. When the etch depth is deeper than the entire slab waveguide thickness, a symmetric waveguide is created and thus the radiation loss is reduced [15, 16].

3. Device Fabrication and Experiments

The integrated receiver as shown in Fig. 1(a) consists of a balanced uni-traveling-carrier photodiode (UTC-PD), a compact 2×2 grating-based beam splitter, and MQW phase modulators. The device is grown on an InGaAsP/InP integration platform with the UTC-PD structure grown above the waveguide. After defining the UTC-PD, deep gratings grooves are formed before the p-cladding and p-contact layer regrowth.

The gratings are patterned on a SiO_2 hard mask using holographic exposure and then transferred to the semiconductor by methane/hydrogen/argon (MHA)-based reactive ion etching (RIE) with hybrid oxygen cycling [17]. The maximal index contrast in the grating region can be achieved by etching the grating grooves through the entire slab waveguide layer. For the slab waveguide thickness used on our integration platform, grating grooves with an aspect-ratio of almost 3 : 1 are needed for an operating wavelength around 1.55 μm. As discussed in the previous section, the deeply etched grating region ensures a minimal total grating length and a low scattering loss. It is also equally important to have a high quality p-cladding regrowth over the grating region to keep the loss low. The fabricated gratings as shown in Fig. 3(b) shows no apparent air voids, which suggests low scattering losses at the regrowth interface. One note worth mentioning is that the grating structure with controlled dimensions is achieved without the need for costly electron beam lithography. It is a robust, well-developed, low cost and high throughput process, and is also compatible with other fabrication steps without obvious additional cost.

To realize our design goals — equal splitting and a short signal path — key design parameters are shown in Fig. 8. The distance between the modulator and the detector is kept the same for all cases and thus the beam divergence is virtually the same. The diverged

beam widths at different propagation distances are arranged to be 3 μm at the input end from the modulator, 10 μm at the grating region, and 12 μm at the detector front end. In order to study the grating reflectivity and mode distortion effects, we investigated a total of nine combinations of three different grating lengths (5 μm, 10 μm, and 15 μm) and three different detector widths (7 μm (S), 12 μm (M), and 23 μm (L)). The middle grating length is selected to match the beam width at the grating region, and the middle detector width is selected to match the beam width at the detector front end. All detectors are 100 μm long, which is sufficient to absorb most of the incident light.

4. Results and Discussion

4.A. Splitting Performance

The peak splitting efficiency at the Bragg wavelength for both the FDTD simulations and experimental data are listed in Table 1 and Table 2. The FDTD simulation data in the case of a time monitor with a width equal to *Det L* are the same as the case of infinite width. Thus the width of *Det L* is considered wide enough to capture all the incoming light and should be independent of mode distortion.

The measured splitting spectra of all nine combinations are shown in Fig. 9 and the peak reflectivity of each case is also plotted in Fig. 10. The splitting ratios of $L_g = 5$ μm and $L_g = 10$ μm cases show little dependence on detector widths. It is very consistent with the simulation results, and it further confirms that the mode distortion has only marginal effects for a thin grating case. On the other hand, when the grating length becomes larger than the interacting beam width, as the case of $L_g = 15$ μm, the measured splitting ratios differ from each other for different detector widths. The beam walk-off effect and the mode distortion are more pronounced in this regime, which results in unequal distortion in transmissive and reflective beams, as explained in [14].

In Fig. 10 we show the well-known tanh-relation [18] between reflectivity and the product of $\kappa \cdot L_g$ with some reasonable assumptions as described below. For an ideal square grating, the reflective coefficient (r_g) and coupling coefficient (κ) can be expressed as follows:

$$|r_g| = \tanh(\kappa \cdot L_g), \tag{2}$$

$$\kappa = \frac{2\Delta n}{\lambda_o}, \tag{3}$$

where Δn is the index contrast between the two alternating layers and λ_o is the Bragg wavelength in vacuum. Here we have made two assumptions to better fit the tanh-curve to

our data:

$$\kappa_{eff} = \eta \cdot \kappa, \qquad 0 \le \eta \le 1 \tag{4}$$

$$|r_g|_{eff} = \alpha \cdot \tanh(\kappa_{eff} \cdot L_g), \qquad 0 \le \alpha \le 1 \tag{5}$$

Eq. (4) assumes the effective coupling coefficient to be η = 77 % of the ideal κ, and Eq. (5) assumes that the reflectivity saturates at α = 80 % of the total incident light. Since the ideal κ is calculated for a rectangular grating profile, the value of η is reasonable when we account for the profile roundup due to processing imperfection such as mask erosion and element exchange during regrowth, as well as the barely etched-through grating grooves. The saturation in the curve for longer gratings can be explained by the fact that the overlap between the grating thickness and the mode profile in the transverse plane is not unity and some parts of the incident wave are transmitted through the deep grating region without experiencing interference [15].

4.B. Insertion loss

The measured insertion loss data shown in Fig. 11 include information about: (1) the propagation loss from the modulator to the detector; (2) the detector mismatch loss; (3) the grating loss. Presumably the propagation loss should be identical in all cases since the waveguide geometry is intentionally kept the same.

If we exclude the mismatch loss for the case of *Det-L* as discussed before, the insertion loss should only include the constant propagation loss and the grating loss. The material propagation loss is measured from a separate measurement to be 0.5 dB, and therefore the grating scattering loss should be not greater than 1.5 dB if the waveguide scattering loss is also taken into account. In this case, the insertion loss only exhibits slight dependence on the grating length within the range of interest. The insertion loss of the grating lengths L_g = 5 μm and 10 μm for the case of *Det-M* are very similar to those of *Det-L*, which implies that most of the incident beams are still within a range equal to *Det-M*. As for the case of L_g = 15 μm, the loss difference between *Det-M* and *Det-L* can be seen as an evidence of mode distortion since some light is not captured by *Det-M* due to mode deformation by the thick grating. Lastly for the case of *Det-S*, another 3 to 4 dB loss for all three grating lengths is observed. Since it is designed to be narrower than the beam width on purpose as explained below, a mismatch-induced excitation loss indeed shows up as expected.

4.C. Extinction ratio

The extinction ratio between the constructive and destructive interferences of two beams that come from the two nominally identical MQW phase modulators is also characterized. The simulated and experimental data of extinction ratios are also shown in Table 1 and Table 2. We can easily see that the case of $L_g = 10$ μm has the greatest extinction ratio among all three grating lengths because of the most equal splitting and therefore best cancelation. The price of the mismatch loss for the case of *Det-S* is paid back in the extinction ratio as it exhibits the greatest extinction ratio among three detector widths. Because the thick grating distorts the transmissive and reflective beams differently, a narrow detector at the center of the beam should only capture the portions that interfere most effectively. This clearly demonstrates the trade-off between mismatch loss and extinction ratio.

According to the discussion above, one may design a compact grating-based beam splitter with a proper choice of detector width to have both low insertion loss and high extinction ratio. As demonstrated in this work, high extinction ratio and low insertion loss as well as nearly equal splitting are achievable with a 10 μm long grating and a 12 μm wide photo detector.

5. Conclusion

In this paper, we present a comprehensive study of a proposed ultra-compact grating-based beam splitter. The fabricated devices experimentally validated our theoretical analysis and simulation data with a high degree of consistency. The design variety of nine different combinations demonstrates the properties of splitting ratio, insertion loss, and extinction ratio. It also provides guidance for a future design. The tradeoff between insertion loss and extinction ratio by varying the detector width is also clear.

An ultra-compact beam splitter with equal splitting, approximately 14 dB extinction ratio, and as low as 2 dB insertion loss has been achieved with only 10 μm long interference region. The grating-based beam splitter is proven to be attractive for compact PICs that require a small loop delay, a minimal device size and low fabrication complexity.

Acknowledgments

This work was supported by DARPA via the PHOR-FRONT program under the United States Air Force Contract. A portion of this work was done in the UCSB nanofabrication facility, part of the NSF funded NNIN network.

References

1. A. Ramaswamy, L. Johansson, J. Klamkin, C. Sheldon, H. Chou, L. Rodwell, M.J. Coldren, and J. Bowers, "Coherent receiver based on a broadband optical phase-lock loop," in "Optical Fiber communication/National Fiber Optic Engineers Conference, OFC/NFOEC," (2007).
2. L. Spiekman, Y. Oei, E. Metaal, F. Green, I. Moerman, and M. Smit, "Extremely small multimode interference couplers and ultrashort bends on InP by deep etching," Photonics Technology Letters, IEEE **6**, 1008–1010 (1994).
3. Y. Ma, S. Park, L. Wang, and S. T. Ho, "Ultracompact multimode interference 3-db coupler with strong lateral confinement by deep dry etching," Photonics Technology Letters, IEEE **12**, 492–494 (2000).
4. C. Janz, B. Keyworth, W. Allegretto, R. Macdonald, M. Fallahi, G. Hillier, and C. Rolland, "Mach-Zehnder switch using an ultra-compact directional coupler in a strongly-confining rib structure," Photonics Technology Letters, IEEE **6**, 981–983 (1994).
5. D. Levy, K. H. Park, R. Scarmozzino, J. Osgood, R.M., C. Dries, P. Studenkov, and S. Forrest, "Fabrication of ultracompact 3-db 2x2 MMI power splitters," Photonics Technology Letters, IEEE **11**, 1009–1011 (1999).
6. C.-C. Chen, H.-D. Chien, and P.-G. Luan, "Photonic crystal beam splitters," Appl. Opt. **43**, 6187–6190 (2004).
7. T. F. Krauss, "Planar photonic crystal waveguide devices for integrated optics," physica status solidi (a) **197**, 688–702 (2003).
8. Y. Zhang, Y. Zhang, and B. Li, "Optical switches and logic gates based on self-collimated beams in two-dimensional photonic crystals," Opt. Express **15**, 9287–9292 (2007).
9. P. Pottier, S. Mastroiacovo, and R. M. De La Rue, "Power and polarization beam-splitters, mirrors, and integrated interferometers based on air-hole photonic crystals and lateral large index-contrast waveguides," Opt. Express **14**, 5617–5633 (2006).
10. Y. Lin, N. Rahmanian, S. Kim, and G. Nordin, "Fabrication of compact polymer waveguide devices using air-trench bends and splitters," in "Southeastcon, 2008. IEEE," (2008), pp. 421–426.
11. Y. Lin, N. Rahmanian, S. Kim, and G. P. Nordin, "Compact and high efficiency polymer air-trench waveguide bends and splitters," (SPIE, 2007), vol. 6462, p. 64620V.
12. C.-H. Chen, M. Sysak, J. Klamkin, and L. Coldren, "Ultra-compact grating-based 2 x 2 beam splitter for miniature photonic integrated circuits," in "Lasers and Electro-Optics Society, 2007. LEOS 2007. The 20th Annual Meeting of the IEEE," (2007), pp. 784–785.
13. C.-H. Chen, J. Klamkin, L. A. Johansson, and L. A. Coldren, "Design and implementation of ultra-compact grating-based 2 x 2 beam splitter for miniature photonic integrated

circuits," in "Optical Fiber communication/National Fiber Optic Engineers Conference, 2008. OFC/NFOEC 2008. Conference on," (2008), pp. 1–3.

14. M. R. Wang, "Analysis and observation of finite beam Bragg diffraction by a thick planar phase grating," Appl. Opt. **35**, 582–592 (1996).
15. J. Ctyroky, S. Helfert, and R. Pregla, "Analysis of a deep waveguide Bragg grating," Optical and Quantum Electronics **30**, 343–358 (1998).
16. M. Palamaru and P. Lalanne, "Photonic crystal waveguides: Out-of-plane losses and adiabatic modal conversion," Appl. Phys. Lett. **78**, 1466–1468 (2001).
17. J. E. Schramm, D. I. Babic, E. L. Hu, J. E. Bowers, and J. L. Merz, "Fabrication of high-aspect-ratio inp-based vertical-cavity laser mirrors using $CH_4/H_2/O_2/Ar$ reactive ion etching," Journal of Vacuum Science & Technology B: Microelectronics and Nanometer Structures **15**, 2031–2036 (1997).
18. S. Corzine, R. Yan, and L. Coldren, "A tanh substitution technique for the analysis of abrupt and graded interface multilayer dielectric stacks," Quantum Electronics, IEEE Journal of **27**, 2086–2090 (1991).

Table 1. FDTD simulations on splitting and extinction ratio.

W_d \ L_g	Rx	Ext	Rx	Ext	Rx	Ext
	5 μm		10 μm		15 μm	
7 μm (S)	21.97 %	10.19 dB	53.86 %	21.15 dB	75.20 %	9.90 dB
12 μm (M)	21.64 %	10.03 dB	51.71 %	17.29 dB	70.71 %	9.53 dB
23 μm (L)	21.62 %	10.00 dB	51.34 %	16.05 dB	68.91 %	8.72 dB

Table 2. Experimental data on splitting and extinction ratio.

W_d \ L_g	Rx	Ext	Rx	Ext	Rx	Ext
	5 μm		10 μm		15 μm	
7 μm (S)	19.52 %	–	50.89 %	18.00 dB	70.25 %	–
12 μm (M)	18.41 %	–	48.03 %	13.88 dB	64.61 %	9.56 dB
23 μm (L)	20.66 %	–	48.98 %	–	57.37 %	7.91 dB

List of Figures

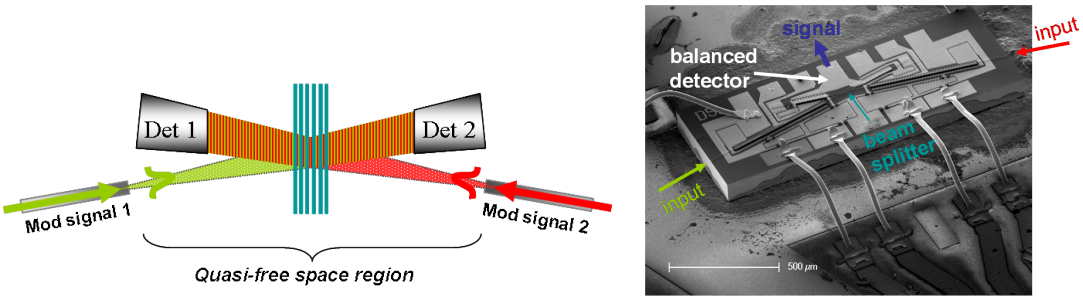

(a) (b)

Fig. 1. (a) Schematic top view of 2×2 grating-based beam splitter which is integrated with two modulators and two photodetectors. Waveguide boundary (not shown) is far away from the diverged beams in the quasi free space region. (b) SEM of integrated compact beam splitter on carrier. Two fiber coupled incoming beams are illustrated with arrows in red and green.

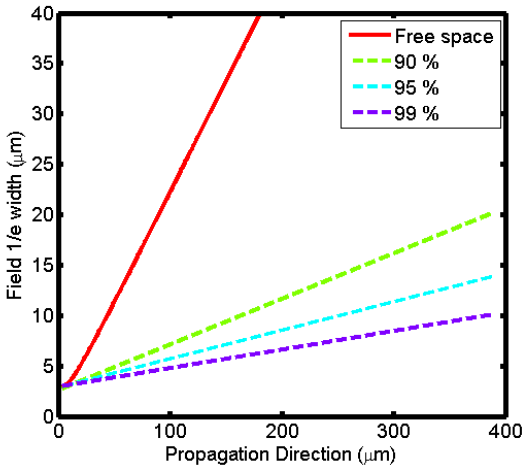

Fig. 2. Comparison of field 1/e width of quasi free space expansion and linear flaring along propagation direction. Different mode expansion speeds in linear flaring give different power transfer percentages (e.g. 90 %, 95 % and 99 %).

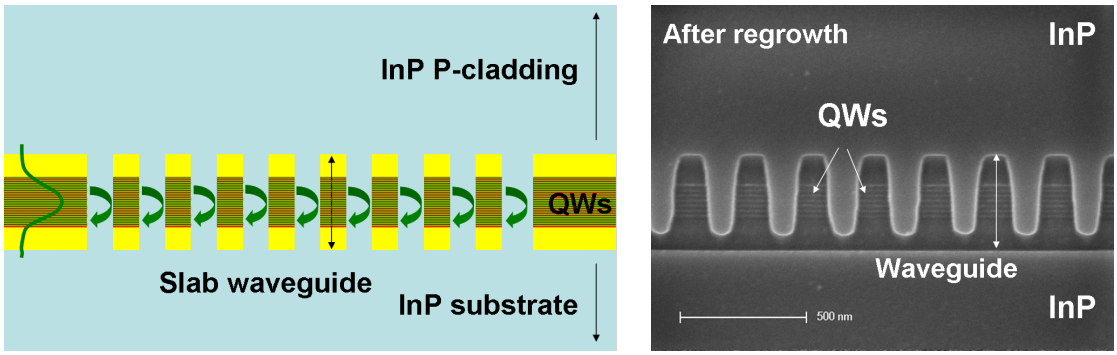

(a) (b)

Fig. 3. (a) Schematic side view of the grating region. The beam is only confined in vertical direction. (b) Regrown gratings cross-section. The slab waveguide layer which contains multiple centered quantum wells can be clearly seen. No obvious air void is observed at the regrowth interface.

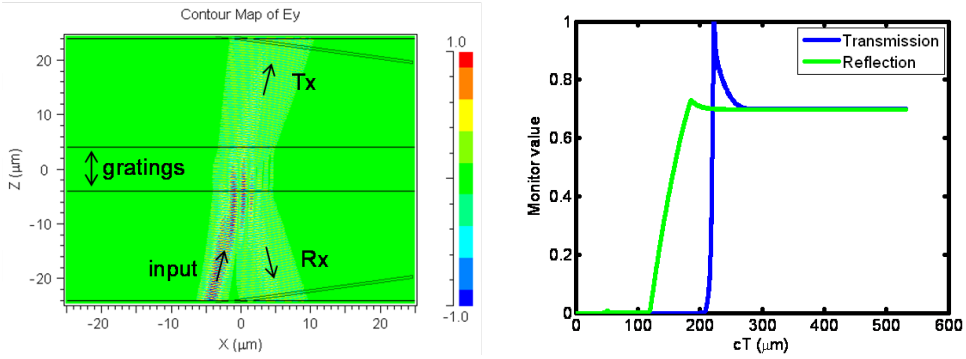

(a) (b)

Fig. 4. FDTD simulation of the Bragg grating splitter with one input at equal splitting condition. (a) FDTD color-coded contour plot of the optical field. (b) Time monitor outputs at transmission and reflection versus time in units of cT (μm) where c is the speed of light in vacuum.

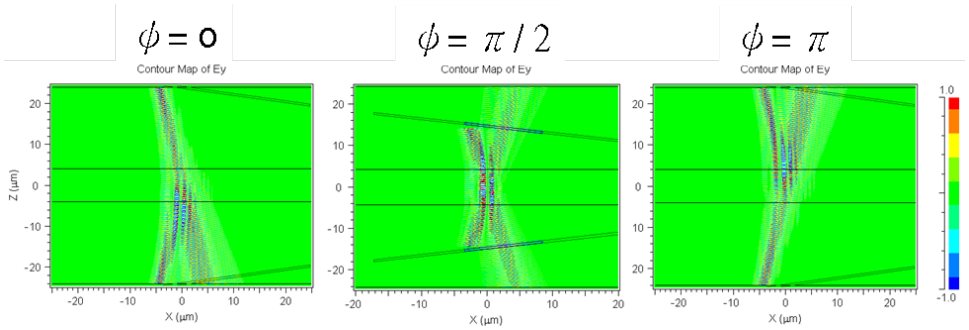

Fig. 5. FDTD simulation of the grating splitter with two inputs in different phase relations.

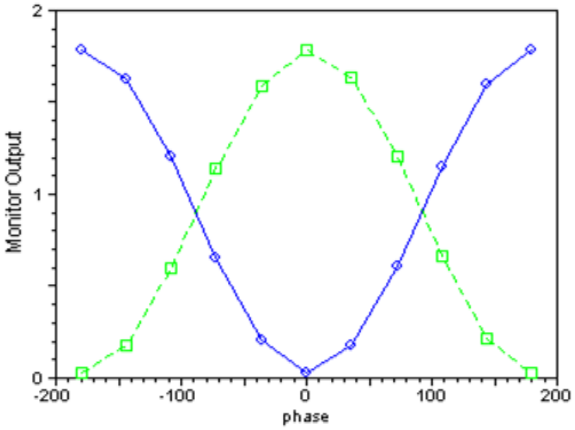

Fig. 6. The simulated power at two output ports versus the phase difference of two inputs. The input power of each beam is set to one.

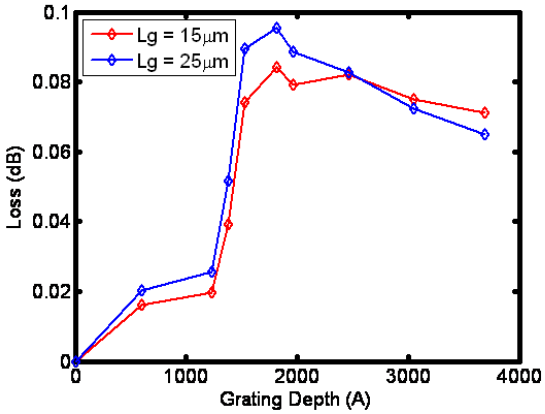

Fig. 7. The FDTD simulated loss versus grating etch depth in the vertical model. Total slab waveguide thickness is 3695 Å.

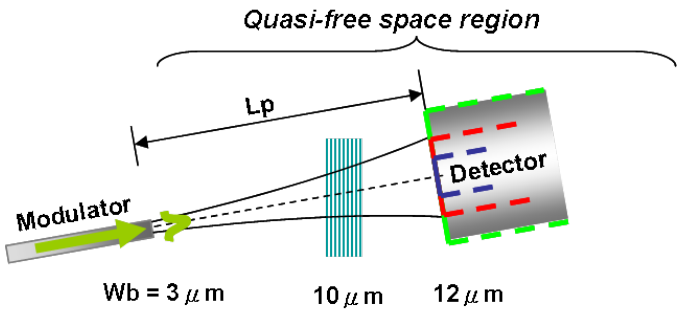

Fig. 8. Beam divergence in the quasi free space region. The beam waist is 3 μm at the input from modulator, 10 μm at the grating region, and 12 μm at the detector front end. Different detector widths are also illustrated in blue (S), red (M), and green (L).

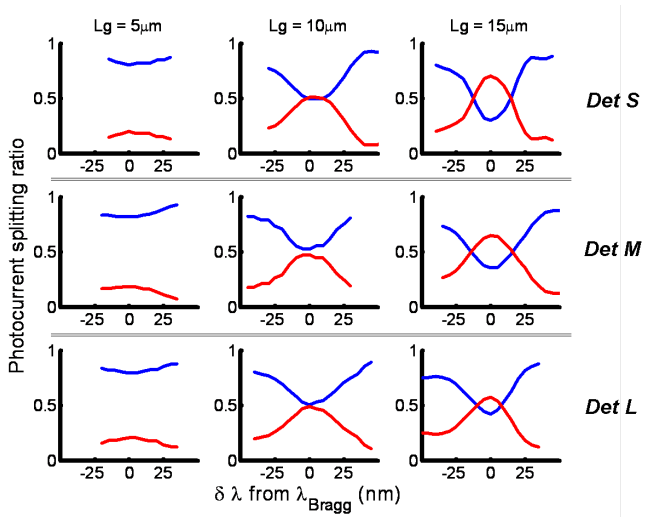

Fig. 9. Measured splitting spectra of nine different combinations with different detector widths and different grating lengths. Red (lower) lines represent the reflection and blue (upper) lines represent the transmission.

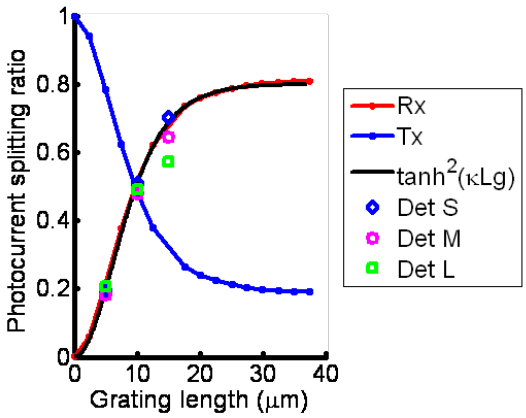

Fig. 10. Photocurrent splitting ratio versus grating length. Lines are from modeling and circles are the measured data.

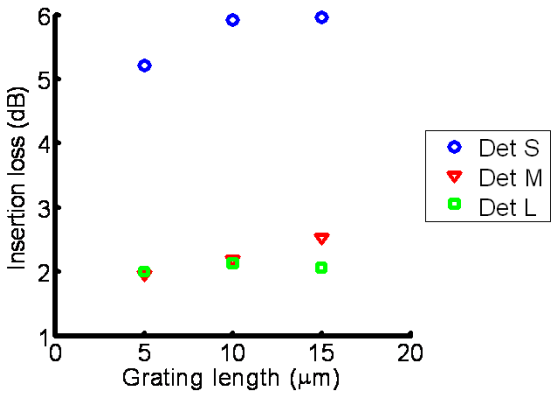

Fig. 11. Measured insertion loss data versus grating lengths.